EUROPEAN ORGANIZATION FOR NUCLEAR RESEARCH

CERN-EP/82-80
18 June 1982

COLLINEAR FAST-BEAM LASER SPECTROSCOPY ON RADIOACTIVE ISOTOPES IN THE RARE-EARTH REGION

Rainer Neugart
CERN, Geneva, Switzerland

Invited paper to the
Conference on Lasers in Nuclear Physics
21-23 April 1982
Oak Ridge, Tennessee, USA

COLLINEAR FAST-BEAM LASER SPECTROSCOPY ON RADIOACTIVE ISOTOPES IN THE RARE-EARTH REGION

RAINER NEUGART
CERN, Geneva, Switzerland

Abstract Collinear-beam laser experiments at ISOLDE have considerably enlarged the range of elements for which hyperfine structures and isotope shifts in long isotopic chains can be measured. The present work aims at a continuation of previous Ba experiments by a systematic study of the transitional region above $N = 82$ in the rare-earth elements. First results have been obtained for the neutron-deficient isotopes of Dy ($146 \leq A \leq 164$), Er ($150 \leq A \leq 170$), and Yb ($156 \leq A \leq 176$) yielding the change of mean-square nuclear charge radii within the isotopic sequences, and the spins, magnetic moments, and electric quadrupole moments for a number of odd isotopes.

INTRODUCTION

The measurement of nuclear ground-state properties by optical spectroscopy came into prominence again when new methods of high sensitivity and resolution gave access to radioactive isotopes far from stability. The pioneering work on the mercury and alkali isotopic chains is covered by special contributions to this conference[1,2]. The aims of this talk are twofold: I shall point out the unique possibilities of collinear fast-beam laser spectroscopy, especially with regard to extensive use with unstable isotopes, and report on recently performed measurements on neutron-deficient isotopes in the heavier rare-earth region.

These studies were initiated by the previous work on neutron-rich Ba isotopes[3]. Together with the results on some very neutron-deficient isotopes and those obtained

by the Karlsruhe group for the longer-lived and stable ones[4], the information on isotope shifts and hyperfine structures covers now the full range between ^{122}Ba and ^{146}Ba. Essentially the same range is known for Cs, partly from collinear-beam spectroscopy at the Mainz reactor[5], and more extensively from the Orsay experiment at ISOLDE[2]. In the two cases, Ba and Cs, the isotope shifts clearly reflect a gradual increase of deformation towards both sides from the magic neutron number N = 82, and in particular close to N = 90.

This latter behaviour is contrary to what is observed for the stable isotopes of the rare-earth elements with the same neutron numbers. More than 30 years ago their isotope shifts had an important impact on nuclear physics. This may justify starting with a historical remark.

The isotope shift of heavy elements, discovered by Schüler and Keyston and by Kopfermann in 1931, was soon recognized as the effect of a change in nuclear volume. Nevertheless, it mainly played the role of an effect disturbing hyperfine structure studies, until Brix and Kopfermann looked systematically at the influence of the electronic structure and thus arrived at more quantitative results on the nuclear properties. In 1949, they published a paper with the title "Zur Isotopieverschiebung im Spektrum des Samariums"[6], in which they presented experimental evidence of nuclear deformation. Collective effects had already been postulated for nuclei with unpaired protons or neutrons, in order to account for the large quadrupole moments observed in a number of cases.

Isotope shifts at that time were measured mainly between doubly-even isotopes, and here a striking irregularity had been discovered already during the thirties. While the components of successive isotopes used to be more or less

equidistant, there was a gap between ^{150}Sm and ^{152}Sm, almost twice as large as the normal separation. Later, the same effect was found between ^{148}Nd and ^{150}Nd. The key to the physics behind it was the observation that these "jumps" occurred between the same neutron numbers N = 88 and N = 90, where there is also a remarkably large increase of the quadrupole moments between the two stable Eu isotopes, ^{151}Eu and ^{153}Eu. Both effects were consistently explained by the assumption of a spheroidal nuclear shape. A simple calculation, based on this model and the shapes suggested by the Eu quadrupole moments, led to a qualitative explanation of the so-called isotope shift constant C_{exp} related to the difference of the mean-square nuclear charge radii $\delta\langle r^2\rangle$.

The increasing confidence in the extraction of these isotope shift constants, based on the comparison of many different transitions, initiated systematic studies of nuclear radii by measuring isotope shifts. Of course, only changes with neutron number were accessible. Therefore, the result remained essentially a one-dimensional picture, pieced together of short isotopic strings along the stability line. Comparisons between different proton numbers were restricted to the few isotonic pairs of isotopes in neighbouring elements.

This situation changed little with the first measurements on isolated long chains of radioactive isotopes. The systematics along Z requires the study of a sequence of elements. The additional knowledge of absolute mean-square radii from muonic X-ray spectra or electron scattering for at least one of the isotopes in each element would even allow a complete two-dimensional mapping of $\langle r^2\rangle$ in the Z,N plane. As long as this information is missing or not accurate enough, one has to rely on auxiliary assumptions, e.g. droplet-model predictions, for the isotonic changes at constant deformation.

The experiments on a few elements in the rare-earth region, recently performed at ISOLDE, represent a first step in this direction. They include the neutron-rich isotopes of Ba as well as the neutron-deficient isotopes of Dy, Er, and Yb, covering roughly the neutron numbers between 82 and 100, and thus including the interesting transitional region from spherical to strongly deformed nuclear shape.

Such a programme requires a versatile tool of sensitive on-line spectroscopy with high resolution. I shall try to show that in this respect the collinear fast-beam laser spectroscopy constitutes a big step forward.

METHOD AND EXPERIMENT

The strength of this method lies in the ideal combination of the concepts of on-line isotope separation and high-resolution laser spectroscopy in fast beams. It solves most of the problems connected with the preparation of samples from the minute amounts of radioactive material in a simple and elegant manner. The remaining limitations on applicability are imposed by the target-ion source performance (i.e. production, release, and ionization efficiency) and by the wavelength range of present cw dye lasers. The beam intensities required at present for an experiment range between 10^4 and 10^7 atoms per second, depending on the strength and hyperfine multiplicity of the optical transition involved. The requirements can now be met at ISOLDE for about 20 elements.

The sensitivity and resolution of the method are based on the phase-space properties of the electrostatically accelerated ion beam. The kinetic-energy spread

$$\delta E = mv\delta v \ ,$$

mainly determined by the ion source, corresponds to a velocity spread δv decreasing in the same proportion as the

velocity $v = (2eU/m)^{\frac{1}{2}}$ is increased. A simple calculation leads to the Doppler width

$$\delta\nu_D = \nu_0 \, \delta E/(2eUmc^2)^{\frac{1}{2}} .$$

With the ISOLDE voltage of 60 kV and typical values of $\delta E = 1$ eV and $\nu_0 = 5 \times 10^{14}$ Hz, one should arrive at $\delta\nu_D = 5$ MHz -- a value which fits well with the natural line width of strong optical transitions. Practical values, including all other sources of broadening, usually lie between 10 and 20 MHz.

Covering the Doppler width by the natural line width means that all atoms in the beam interact with the resonant laser light and thus contribute to the fluorescence signal. This is an important condition for high sensitivity. High light-collection efficiency and low background are the remaining and somewhat contradictory crucial points. The background may originate from scattered laser light (especially if the fluorescence wavelength cannot be separated from the laser wavelength by optical filters), collisional excitation, and radioactivity.

An important feature is the variety of states in which the fast beam can be prepared. Ions emerging from the ion source are predominantly in the ground state. For a few cases it has been shown that long-lived excited states can be populated strongly enough so that laser excitation to higher levels becomes possible[7]. Neutralizing the beam by charge-transfer reactions

$$B^+ + A \rightarrow B + A^+ + \Delta E$$

leads to the spectra of neutral atoms that tend to be more easily accessible to cw laser radiation than the ionic spectra. The choice of the reaction partner A gives the possibility of influencing the final-state distribution

and can lead to a predominant population of either the atomic ground state or metastable states, to be used for laser excitation. This is illustrated for the example of Yb in a separate contribution to this conference[8]. It is of major importance that the charge-transfer cross-sections ($\gtrsim 10^{-15}$ cm^2) are usually so large that the phase-space distribution of the beam, and thus the velocity spread, remains nearly unchanged.

For a specific experiment, the atomic transition has to be selected taking into account the wavelength, hyperfine multiplicity, and oscillator strength, as well as optical pumping processes, so as to ensure the highest possible sensitivity and to obtain the most conclusive information on the nuclear parameters. Very often the solution may be a compromise between both. In the experiments discussed here, we have chosen various transitions in the spectra of the neutral atoms, starting either from the ground state or from metastable states.

Experiment

Figure 1 shows the experimental set-up in a somewhat simplified scheme. Not shown is the ISOLDE isotope separator, which should be seen as an integral part of the apparatus -- interlinked with the experiment in many respects.

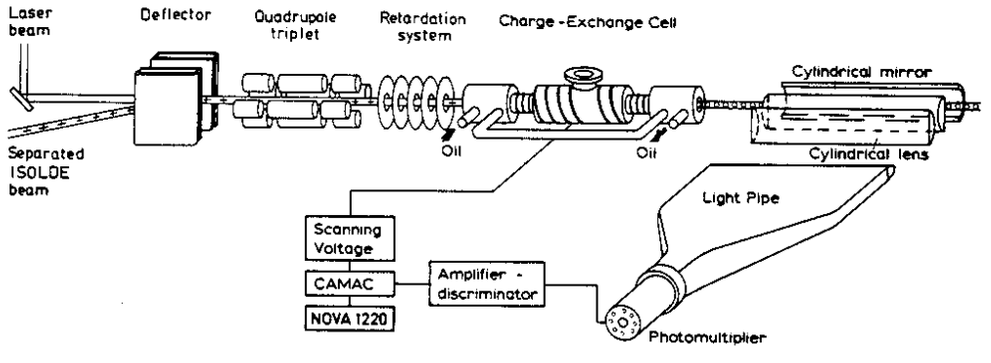

FIGURE 1. Set-up for on-line collinear-beam laser spectroscopy.

COLLINEAR FAST-BEAM LASER SPECTROSCOPY

The beam axis is defined by the laser beam, and the alignment for collinear geometry is accomplished by electrostatic deflection of the ion beam. Both beams have a waist of about 3 mm diameter in the observation region. The charge-exchange cell contains alkali vapour at a pressure of about 10^{-3} Torr. The exact vapour pressure depends on the specific reaction and is usually chosen to neutralize 50% to 70% of the ions. This upper limit is given by the cross-section of secondary collisional excitations involving energy loss and thus broadening the velocity distribution.

An acceleration or deceleration voltage of between -10 kV and +10 kV is applied to the charge-exchange cell for Doppler tuning. Thus the frequency of the laser radiation in the rest frame of the atoms can be changed by about 100 GHz, and if transitions of different isotopes are compared their velocity difference according to the atomic masses can be compensated. This offers the possibility of taking spectra from different isotopes at fixed laser frequency and of calibrating the frequency scale by precision measurements of the voltages.

An example of such a measurement is shown in Figure 2. The two stable even isotopes ^{158}Dy and ^{156}Dy and the radioactive odd isotope ^{151}Dy were alternately directed through the apparatus, and the spectra were taken by multichannel photon counting with convenient voltage sweeps for each of the isotopes in a fast cyclic measuring sequence. The first-order expression for the corresponding frequency shifts,

$$\nu_2 - \nu_1 = \nu_0\left[(2eU_1/m_1c^2)^{\frac{1}{2}} - (2eU_2/m_2c^2)^{\frac{1}{2}}\right] ,$$

shows that the voltages as well as the atomic masses enter into the calculation. We made no attempt to eliminate or measure the masses since the available measured values tend to be

much more precise than needed here, and even the values calculated from systematics seem to be reliable enough.

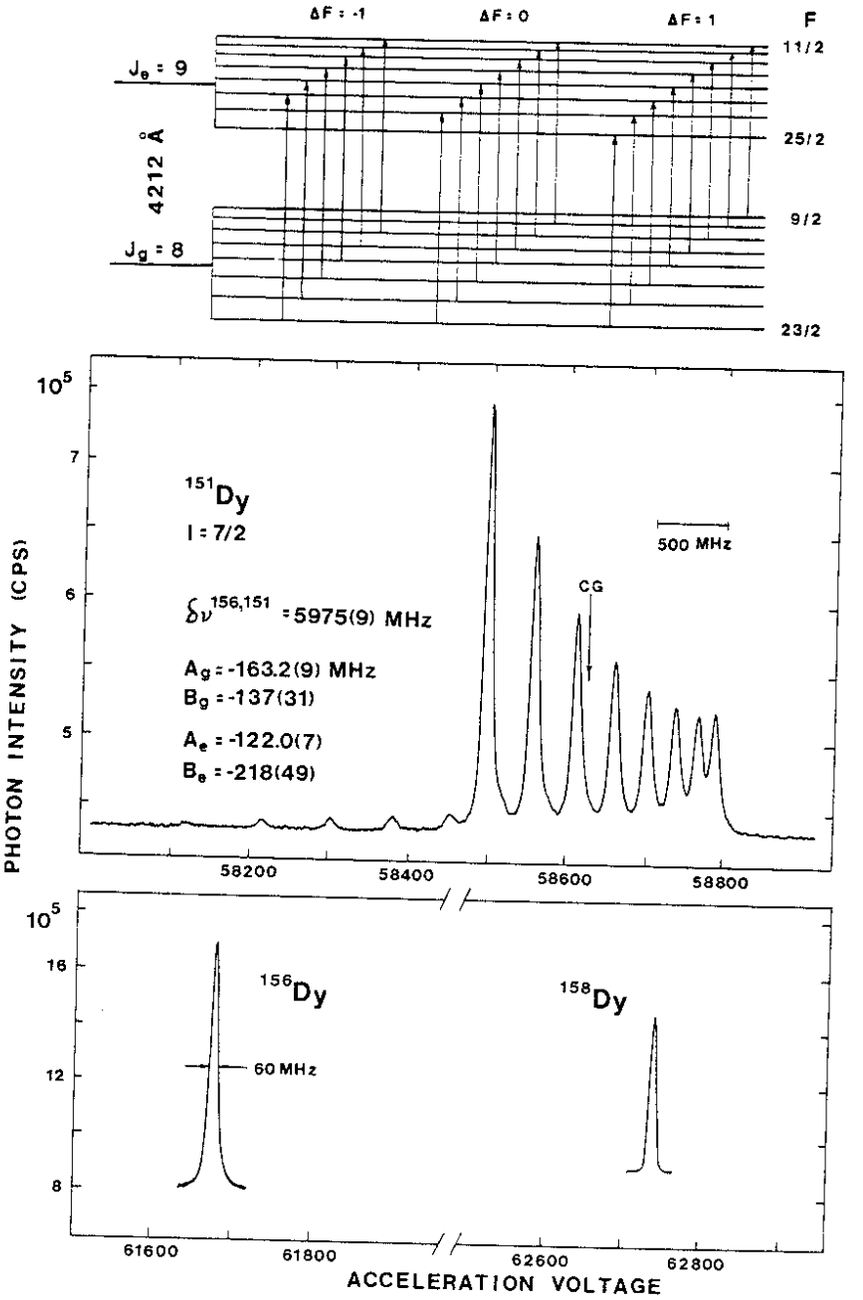

FIGURE 2. Example of a measured spectrum for ^{151}Dy, with the stable reference isotopes ^{156}Dy and ^{158}Dy. The level scheme of the odd isotope is given at the top. The number of hyperfine components (of which only the strong $\Delta F = 1$ and weak $\Delta F = 0$ transitions are seen) is determined by the nuclear spin.

COLLINEAR FAST-BEAM LASER SPECTROSCOPY

Before turning to the nuclear-physics results, we should discuss some more specific points of the rare-earth experiments, mainly concerning the isotope production and the atomic spectra. In both respects there are striking similarities within this group of elements, very much facilitating the technical aspects of a systematic study.

Production of the Beams

The simultaneous production of the beams of radioactive rare-earth isotopes is favoured by their similar chemical behaviour. The spallation of ^{181}Ta, induced by 600 MeV protons from the CERN Synchro-cyclotron, leads to an efficient production of the neutron-deficient nuclides in the heavier rare-earth region. We used a modified version of the target - ion source system described by Ravn[9]. The target material consists of rolled Ta foils heated to 2200 °C, which gives an efficient release of almost all elements between Sm and Lu [10]. The yields of Dy, Er, and Yb, normalized to 1 μA proton-beam intensity, are displayed in Figure 3. They are measured by β- and γ-ray spectroscopy, and relative measurements by laser spectroscopy have been used to complement the curves for the elements considered here.

The isobars of the different elements are of course simultaneously present in the mass-separated beams. This would be a serious drawback for all experiments using nuclear radiation, but does not disturb atomic-resonance spectroscopy, apart from some background problems. The high radioactivity level and the decay of long-lived atomic states populated in the charge-transfer process give rise to high count rates from the photomultiplier, even in measurements on very weak isotopic components of the element under study.

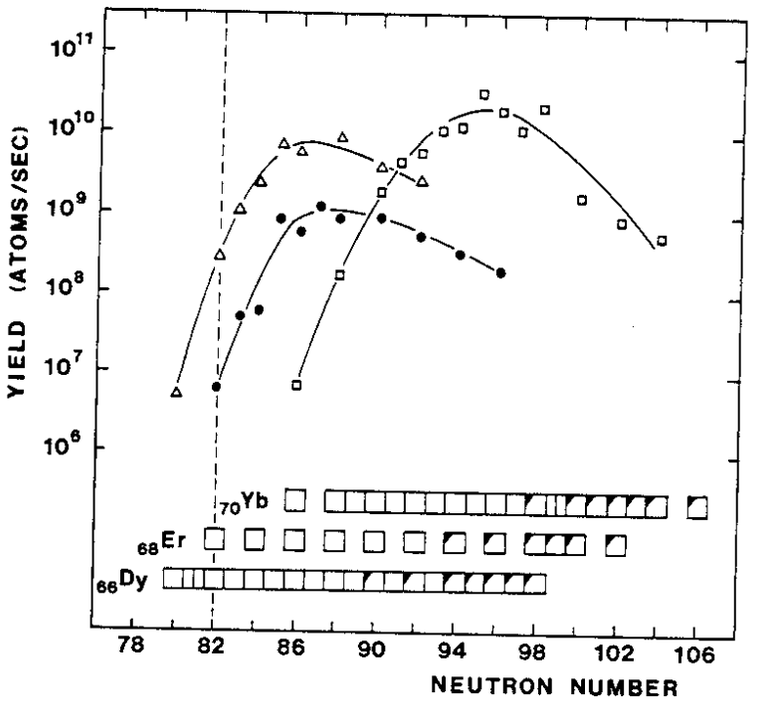

FIGURE 3. Maximum production yields of the neutron-deficient Dy, Er, and Yb isotopes from a Ta-foil target, normalized to a proton-beam intensity of 1 μA. The yields were partly lower during the measurements, although a proton beam of 2 μA was used. The isotopes studied are indicated at the bottom, and stable isotopes are marked with a full triangle.

Spectra of 4f-Shell Atoms

The atomic spectra in the series of elements between Ba and Yb are based on a $6s^2$ valence-electron configuration in the ground state and the open 4f shell. Only Ba (with empty 4f shell) and Yb (with filled 4f shell) have simple two-electron spectra differing essentially only in the energy scale. The strong resonance transition $6s^2\ ^1S_0 \rightarrow 6s6p\ ^1P_1$ has a convenient wavelength of 5536 Å for Ba, but lies at 3988 Å -- beyond the reach of present single-mode dye lasers -- for Yb.

The weak intercombination line $6s^2\ {}^1S_0 \rightarrow 6s6p\ {}^3P_1$ at 5556 Å involves disadvantages for the sensitivity. The use of transitions from metastable states as a way out of this problem is discussed in the contribution by Klempt et al.[8]

The complex spectra of the rare-earth elements in the proper sense, and Dy and Er in particular, can be understood as the result of an additional coupling of the $6s^2$ valence-electron pair with the $4f^n$ core, yielding a large number of states and transitions (Fig. 4). We still find the basic features of a two-electron spectrum: for example, the ${}^5I_8$ ground state of Dy can be described as $4f^{10}({}^5I_8)6s^2({}^1S_0)\ {}^5I_8$.

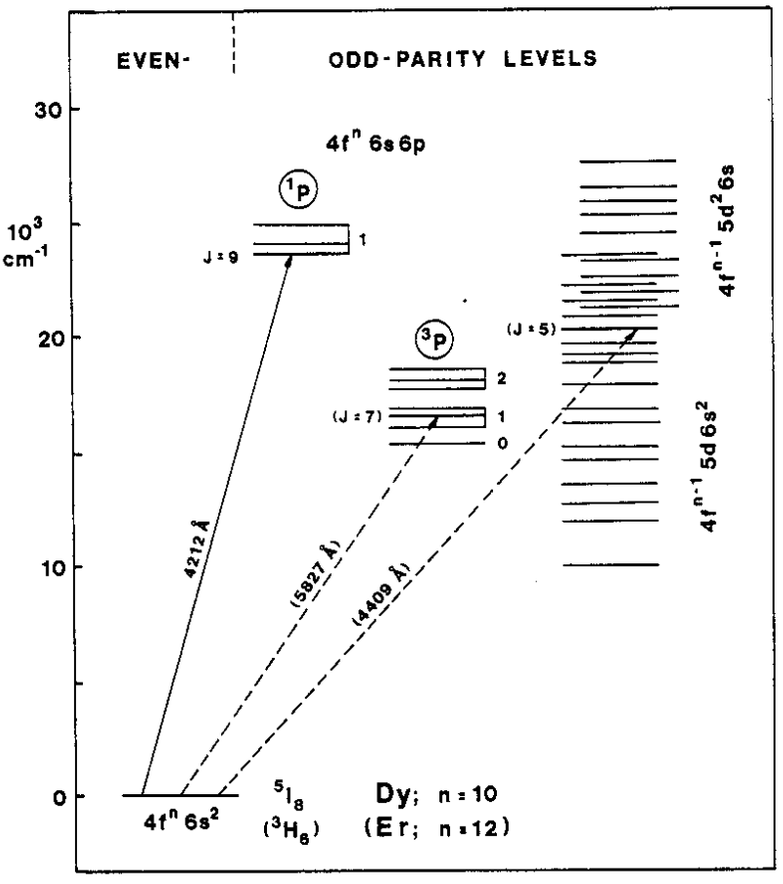

FIGURE 4. Simplified level diagram of Dy (Er). The arrows indicate the transitions used. The energy scale is correct for both elements within about 10%.

Strong resonance lines in the deep blue lead to the configuration $6s6p(^1P_1)$ with unchanged core and three possible values of the total angular momentum, J = 7, 8, 9. The weak transitions to $6s6p(^3P_{0,1,2})$ are analogous. In addition, there are a large number of states described by f^9ds^2, connected with the ground state by transitions of various strengths. The coupling scheme, presented here, can of course only serve as a guide and is subject to strong configuration mixing.

For our purpose, considerations on sensitivity clearly favour the $s^2 \rightarrow sp$ transitions to the $^1P_1$ configuration. They should also give reliable information on the mean-square nuclear charge radii from the isotope shifts. Therefore we have chosen the transition

$$4f^{10}(^5I_8)6s^2(^1S_0)\ ^5I_8 \rightarrow 4f^{10}(^5I_8)6s6p(^1P_1)\ , \quad J = 9$$

at 4212 Å for the Dy experiment.

The isotope-shift and hyperfine-structure measurements performed so far cover all even and odd isotopes in the sequence between ^{146}Dy and ^{164}Dy, and include the high-spin isomer of ^{147}Dy. All measured hyperfine components and their centres of gravity are shown in Figure 5. The hyperfine structures exhibit a distinct change between the sequence of the almost spherical I = 7/2 isotopes and the I = 3/2,5/2 deformed ones. As expected, the trend of the isotope shifts shows a kink at the magic neutron number N = 82, and a step between N = 88 and N = 90 due to the onset of a large static nuclear deformation. We shall go into further comparisons and discussions of this behaviour in the context of the nuclear properties extracted and especially their dependence on the proton number.

A less favourable situation is found in the Er spectrum, where the strong transitions to the configuration $f^{12}(^3H_6)$ $6s6p(^1P_1)$ appear shifted further to the blue, and their

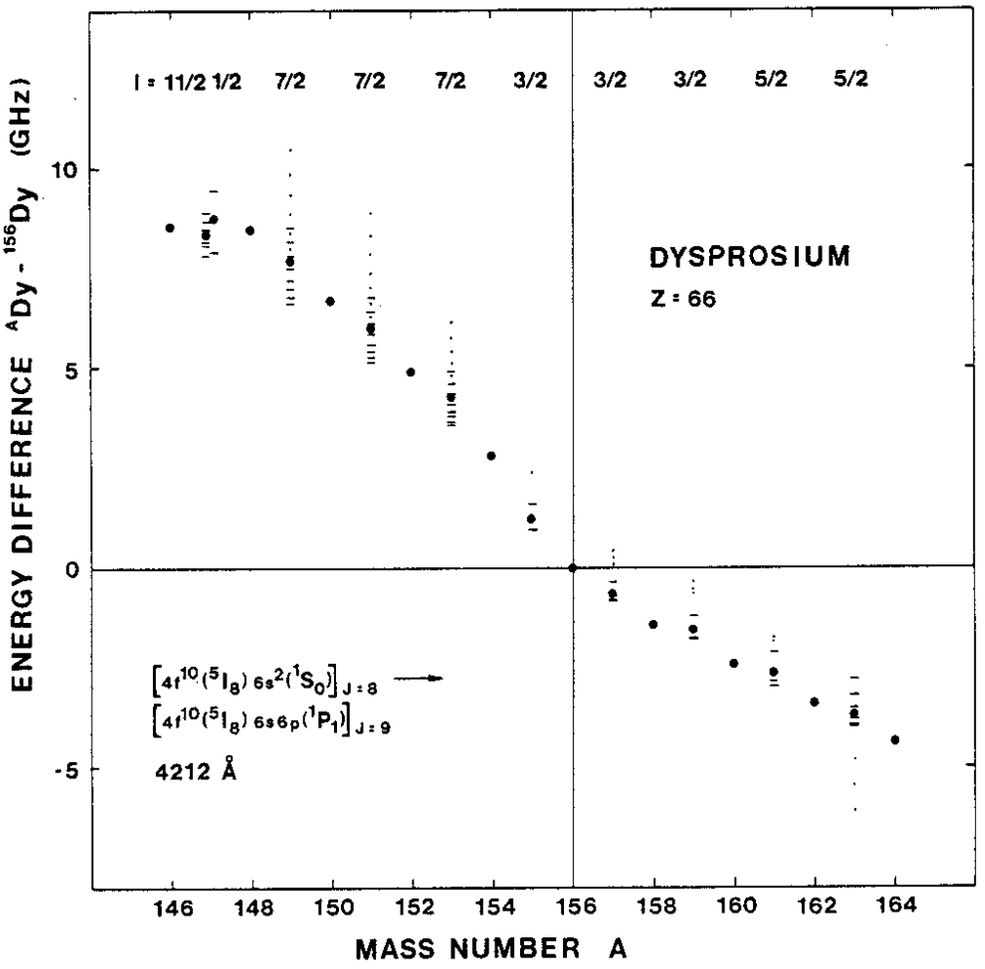

FIGURE 5. Observed hyperfine components of the Dy isotopes, with respect to ^{156}Dy. The centres of gravity are shown by full circles. Dashes and small dots represent the $\Delta F = 1$ and $\Delta F = 0$ transitions, respectively.

isotope shifts seem to be strongly reduced by admixtures of $f^{11}ds^2$ configurations. This led us to the choice of the transition to $f^{12}(^3H_6)6s6p(^3P_1)$, $J = 7$ at the convenient wavelength of 5826 Å, for a few isotopes at the top of the yield curve. An extension of the studies to some less abundant isotopes could be made in one of the strongest transitions of the type $f^{12}s^2 \rightarrow f^{11}ds^2$ (4409 Å), which have large negative field shifts. The connection between both lines, made in a King

plot, requires the inclusion of neutron-deficient isotopes because of the almost equidistant line positions in the range of stable isotopes. The complication from hyperfine structures has been circumvented at this stage, and present data include the sequence of even isotopes from ^{150}Er to ^{170}Er ($82 \leq N \leq 102$).

DISCUSSION OF NUCLEAR PHYSICS RESULTS

For the moment, let us omit the problems involved in the extraction of the nuclear quantities from the observed atomic spectra. We shall come across them in a number of details of the results discussed in the following.

Mean-Square Charge Radii and Deformation

Atomic spectroscopists are familiar with the type of diagram presented in Figure 6 and originally introduced by Brix and Kopfermann as a clearly arranged compilation of nuclear physics information from optical isotope shifts. It shows the change of mean-square charge radii between isotopes of neutron numbers N - 2 and N. As a differential plot, it is suitable for illustrating details and irregularities, apart from the odd-even effect.

In the present plot, the curve of Dy represents essentially what is known from the sequence of stable isotopes in Ce, Nd, Sm, and Gd: for example, the "jump" between N = 88 and N = 90. For the sake of clarity, these old data have been omitted in the figure. It is obvious that the peak disappears gradually in the sequence Dy, Er, Yb, as well as for Ba which has 4 protons less than Nd -- the lightest element for which the effect has been observed. It is thus localized to a relatively narrow range of proton numbers around, say, Z = 64, and we shall have to interpret it as a proton-subshell effect.

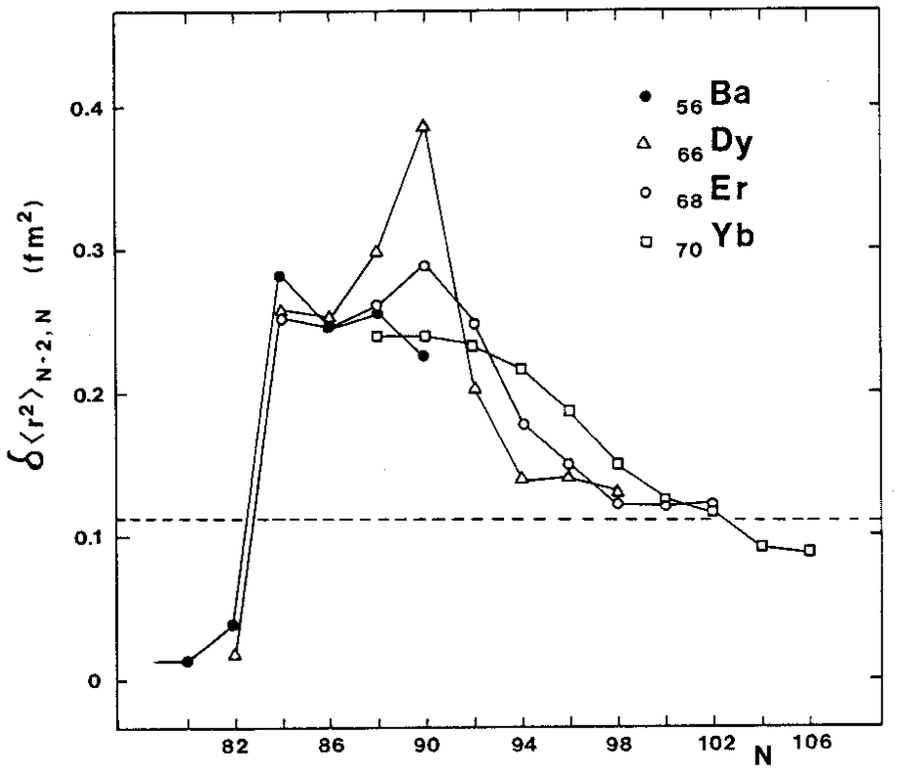

FIGURE 6. Brix-Kopfermann diagram for the differences of mean-square charge radii between isotopes N - 2, and N. The horizontal dashed line corresponds to the spherical droplet model.

The overall trend of the radii is believed to be mainly determined by deformation effects, apart from a regular increase with neutron number to be described, for example, by the droplet model[11]. According to the formula

$$\langle r^2\rangle = \langle r^2\rangle_0 + \frac{5}{4\pi}\langle r^2\rangle_0 \langle\beta^2\rangle$$

the deviations from the spherical $\langle r^2\rangle_0$ can be ascribed to the mean-square deformation $\langle\beta^2\rangle$. The latter decreases

with neutron number below the neutron-shell closure and increases above, leading to the dramatic change of the magnitude of $\delta\langle r^2\rangle$ at N = 82. For Yb, the plot clearly suggests a smooth transition to the strongly deformed isotopes, with a maximum of $\langle\beta^2\rangle$ reached around N = 100, whereas for Dy (as well as for Gd, Sm, and Nd) the onset of strong deformation occurs essentially in one big step at N = 90.

The overall trends are better seen in a plot of the integral mean-square charge radii shown in Figure 7, which includes the data on odd isotopes. For adequate comparisons the differences of $\langle r^2\rangle$ from the isotopes with a closed neutron shell are displayed. Also shown is the slope of the line corresponding to the droplet model with equi-deformation lines according to the equation above. With the assumption $\langle\beta^2\rangle^{\frac{1}{2}} = 0.1$ for N = 82 nuclides, suggested by B(E2) values, the strongly deformed isotopes end up at deformations slightly larger than 0.3 consistent with other information from nuclear spectroscopy, especially the B(E2) values, and with the quadrupole moments discussed below.

In this preliminary evaluation of $\delta\langle r^2\rangle$ from the measured isotope shifts we have followed the procedures suggested for these elements by Heilig and Steudel[12]. In view of the comprehensiveness and the accuracy of the new data, the uncertainties involved of course require careful reconsideration, in particular for the influence of configuration mixing on the field shifts of the assumed pure $s^2 \rightarrow sp$ transitions. Nevertheless, the results seem to be quite consistent among themselves and with the overall trend of nuclear behaviour extracted from nuclear spectroscopy.

Nuclear Spins and Moments of the odd Isotopes

While the isotope shifts are well described by nuclear properties of collective nature, the spins and magnetic moments

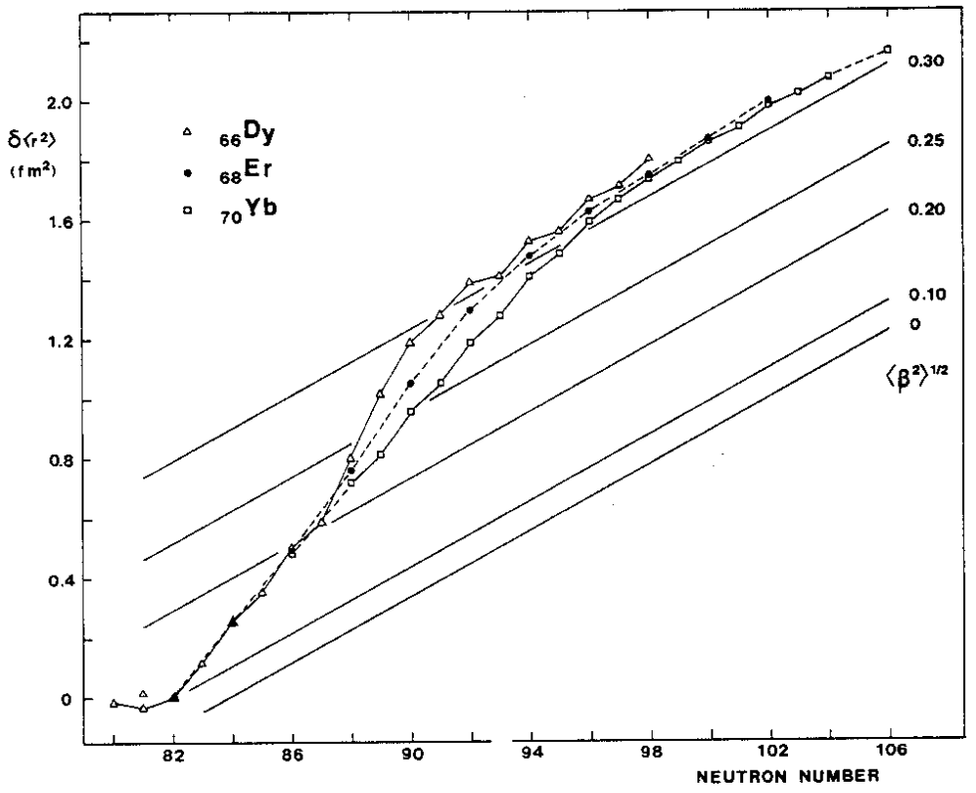

FIGURE 7. Integral change of mean-square charge radii, with respect to the isotopes with N = 82. The slope of the equi-deformation lines is given by the droplet model.

of the odd isotopes reflect single-particle aspects. The spectroscopic quadrupole moments may be seen as the result of an interplay between both. A consistent theoretical description should include spherical as well as strongly deformed nuclei, and especially account for the complex situation in the transitional region. The particle-rotor approach by Larsson et al.[13] has been quite successful in carrying out this task for various regions of the chart of nuclides[14]. It is based on a Nilsson-model description, taking into account also non-axial shape degrees of freedom

and a number of orbitals close to the Fermi level that are available to the odd particle.

The new information on nuclear spins and moments covers essentially the odd Ba, Dy, and Yb isotopes in the transitional region above N = 82. I shall not aim at a comprehensive presentation of the data, but rather give a few examples in comparison with the result of model calculations made by C. Ekström.

The spin I = $^7/_2$ for the ground states of odd-neutron nuclei above the N = 82 neutron-shell closure is readily accounted for by the $f_{7/2}$ shell-model state. It is found in Ba and Ce for N = 83, in Nd for N = 83 and 85, and in Sm, Gd, and Dy for N = 83, 85, and 87. Within the particle-rotor model, the range N = 83 to 87 is described by a successive filling of the sublevels from the $f_{7/2}$ shell, corresponding to the increasing energies of the Fermi levels, as shown in Figure 8. This leads to a qualitative description of the magnetic moments and the spectroscopic electric quadrupole moments, reproducing in particular the trend of negative to zero quadrupole moments.

It should be pointed out that the ground-state properties of these weakly deformed nuclei can only be reproduced by a parameter set for the Nilsson potential, which is different from that commonly used in the strongly deformed rare-earth region. The present values are adapted to the single-particle levels in the spherical limit[15], resulting in an increase of the energy of the $h_{9/2}$ shell and thus a reduction of the mixing into $f_{7/2}$.

All rare-earth nuclei with N $\geq$ 91 belong to a region of strong nuclear deformation. Their ground states are described by essentially pure Nilsson-model orbitals. In Figure 9, a comparison is shown between the experimental nuclear moments

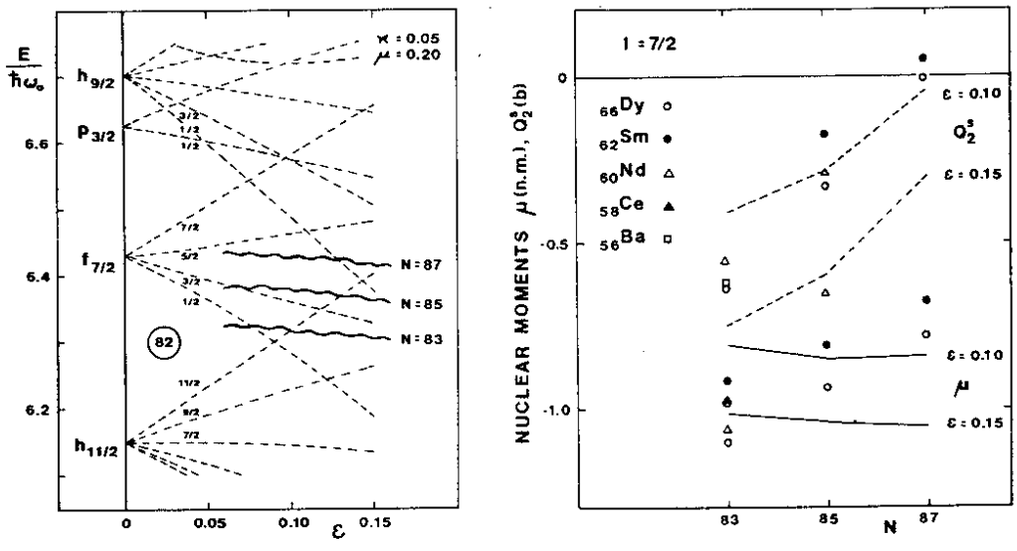

FIGURE 8. Nilsson diagram for odd neutrons in the N = 82 region, with the Fermi levels for N = 83 to 87. A comparison between experimental and theoretical nuclear moments of spin I = $^7/_2$ ground states is given on the right. The theoretical curves are shown for ε = 0.1 and 0.15 ($\beta = 1.06\varepsilon$).

of odd-neutron nuclei with N = 91 to 97 and theoretical values calculated within the particle-rotor model using the "A = 161" potential parameters[16].

The Z = 64 Proton Subshell Closure

Let me summarize the global features of our results:

i) For the elements between Z = 56 and 70 the isotope shifts indicate a similar increase of mean-square radii above N = 82, ending with a large step into strong deformation between N = 88 and 90 for Nd, Sm, Gd, and Dy, but continuing smoothly for Ba and Yb. Er and probably Ce play the role of intermediate cases.

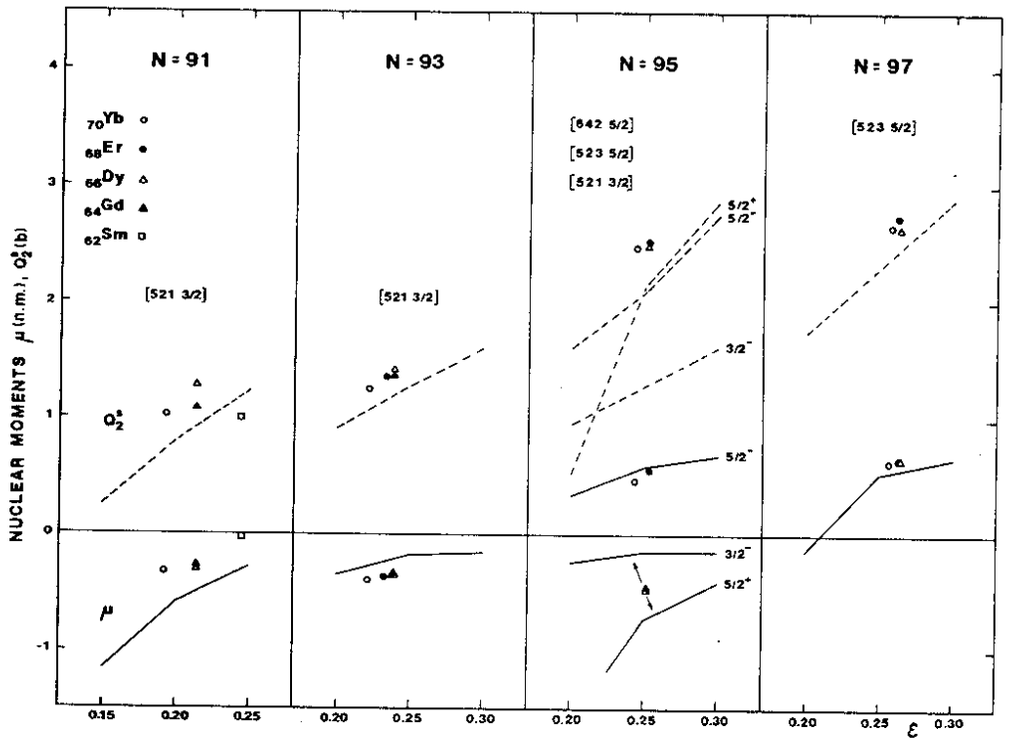

FIGURE 9. Comparison between experimental and theoretical nuclear moments of odd-neutron nuclei in the range N = 91-97. The experimental values are given at the calculated equilibrium deformation positions[16]. The dominant Nilsson orbital is given at the top.

ii) Correspondingly, the single-particle structure of the odd isotopes between N = 82 and 88 for the elements around Z = 64 is associated with more or less pure $f_{7/2}$ shell-model states, while that of the heavier isotopes requires a description in terms of deformed nuclear shapes.

The key to a general interpretation of this behaviour seems to be the proton-subshell closure at Z = 64 and its effect of stabilizing spherical nuclear shapes. A naïve picture would suggest the steepest increase of deformation

in the middle between the closed proton shells at Z = 50 and 82, i.e. around Z = 66. This trend is counteracted by the subshell closure at Z = 64, leading to equi-deformation curves almost parallel to the Z axis and thus explaining the similarity in the behaviour of $\delta\langle r^2\rangle$ close to N = 82 within the full sequence of elements. Since Z = 64 looses its significance as a magic proton number for large deformation, the bistability of nuclear shape around N = 88 to 90 leads to a situation similar to that which has been observed in the light Hg isotopes. For N > 90, the continuation of $\delta\langle r^2\rangle$ curves follows the behaviour expected around the centre of a region of strong deformation.

These observations are in agreement with the results of a recent analysis of the energies of 2^+ and 4^+ states in the ground-state vibrational/rotational bands[17].

Apart from this global view, the present results allow a rather detailed examination of the nuclear structure in this transitional region. In particular, the open question of a quantitative interpretation of the so-called odd-even staggering should be a challenge for nuclear theoreticians.

Problems of Data Analysis

The accuracy of present-day isotope-shift and hyperfine-structure measurements as well as the largely increased range of investigation has caused a strong demand for a better knowledge of the atomic structure parameters entering into the evaluation of the nuclear properties. This problem concerns mainly the mean-square charge radii from isotope shifts and the spectroscopic quadrupole moments from hyperfine structures.

Experimental and theoretical efforts are being made at present to improve the basis of this procedure[18]. Wherever possible, comparisons should be made with the results of

muonic X-ray isotope-shift and hyperfine-structure measurements. The progress of this technique in improving the measuring accuracy and the theoretical basis of analysing the data gives good hope that an accurate calibration of the electronic parameters will be feasible in a number of cases[19]. In addition, the comparison between isotope-shift data of different elements requires accurate absolute mean-square radii that can be expected from the combined analysis of muonic isotope shifts and electron scattering.

The two different approaches -- atomic structure calculations and muonic data -- should remain complementary sources of information leading to a consistent picture. By no means will the spectroscopy on muonic atoms be able to give conclusive information if less than three stable isotopes can be studied, and even for longer strings of stable isotopes the separation of field-shift and mass-shift contributions requires irregular changes of the nuclear radii.

Figure 10 should be seen as an illustrative example of the problems discussed above. It aims at a presentation of $\langle r^2 \rangle$ in the region covered by the experiments discussed here. The values available for $\langle r^2 \rangle$ from muonic atoms or electron scattering[20,21] are combined with the $\delta\langle r^2 \rangle$ from optical isotope shifts. For consistent presentation, all isotope-shift data are calibrated according to Heilig and Steudel[12]. The errors originating from the different pieces of information are omitted.

Although this plot seems to reproduce fairly well the global behaviour of nuclear radii, a few inconsistencies in details are obvious: the increase of the radii along the chain of N = 82 isotopes should be more regular than suggested by the extrapolation from the range of stable isotopes, and roughly follow the droplet-model prediction. Reasons for this can be found in the points made above:

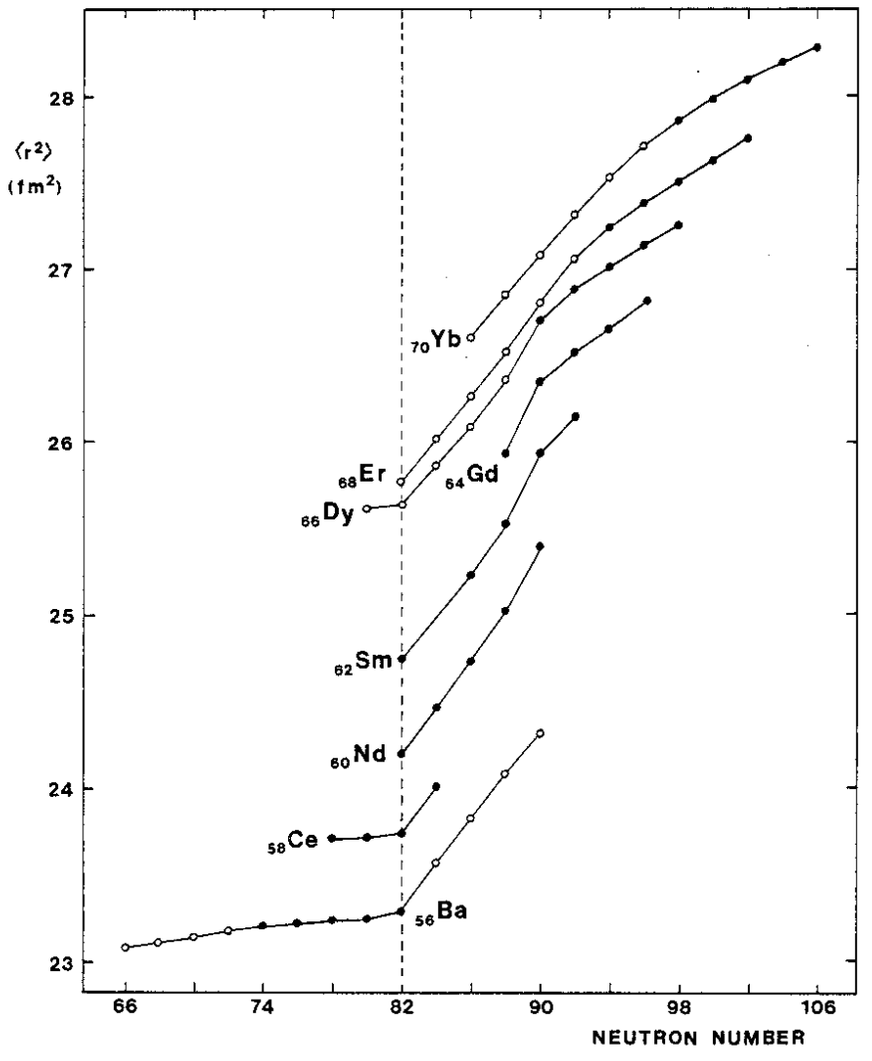

FIGURE 10. Tentative plot of $\langle r^2 \rangle$ in the rare-earth region. The absolute values are taken from muonic spectra[20] or electron-scattering experiments[21] on stable isotopes, and optical isotope shift data[12] for $\delta\langle r^2 \rangle$ are used within isotopic chains. The new data are represented by open circles.

i) The absolute values of $\langle r^2 \rangle$ are not accurate enough for this kind of comparison between different elements. They scatter considerably in the cases where several values can be found in the literature.

ii) The long isotopic strings now accessible to optical measurements require a more reliable procedure of calculating $\delta\langle r^2\rangle$.

In a way, plots such as the one shown in Fig. 10 may reveal the insufficiencies of the data and give hints of a carefully directed improvement. The present generation of muonic-atom-spectroscopy and electron-scattering experiments should overcome one part of this problem [(i) above] to a large extent. It is less obvious whether the calibration of $\delta\langle r^2\rangle$ from optical isotope shifts will reach the desired 1% accuracy level.

EXPERIMENTAL PROSPECTS

I have presented a series of recent experimental results of collinear fast-beam laser spectroscopy at the on-line isotope separator ISOLDE at CERN. They have shown the possibility of studying nuclear charge radii and moments, not only in isolated isotopic strings but also for a number of neighbouring elements in regions of special interest for nuclear physics. By introducing the proton number as an additional parameter, this gives a new quality to the data.

The technique in its original version[22,23] has proved to be sensitive enough for typical ISOLDE beam intensities, ranging from 10^7 to 10^{10} atoms per second for the flat top of the yield curves. On the other hand, isotopes very far from stability as well as quite a number of elements are less favourably produced. Therefore an increase of the sensitivity -- about 10^4 atoms per second have been sufficient for a measurement in the best case, but 10^6 atoms per second may be a more representative number -- will remain a challenge.

The effort in this direction includes more efficient light-collection systems and a reduction of background, as

well as the use of non-optical detection schemes. In the latter respect, ionization spectroscopy -- including ion counting -- may lead to a high detection efficiency. Laser excitation to auto-ionizing states or Rydberg states may be facilitated by charge exchange into metastable states, from which the ionization limit can be reached by a two-step process. A different scheme of ionization, circumventing the problem of low photo-ionization cross-sections that require high cw laser power, is being studied at present for the noble gases. It exploits the differences in cross-sections for collisional ionization between atomic ground states and metastable states, and may be used to detect a change of the respective populations introduced by optical pumping. The first results are promising. They may lead to an extension of the present studies to the neutron-rich Xe isotopes.

Acknowledgements

This talk is based on the results obtained by a group which is identical to the authors of refs. 3 and 8. In addition to them, I would like to thank H.L. Ravn and the ISOLDE Target Group for their expert help.

REFERENCES

1. H.-J. Kluge, Invited paper, these proceedings.
2. C. Thibault, Invited paper, these proceedings.
3. R. Neugart, F. Buchinger, W. Klempt, A.C. Mueller, E.W. Otten, C. Ekström and J. Heinemeier, Hyperfine Interactions, 9, 151 (1981);
   A.C. Mueller et al., to be published.
4. H. Rebel and G. Schatz, Invited paper, these proceedings.
5. J. Bonn, W. Klempt, R. Neugart, E.W. Otten and B. Schinzler, Z. Phys., A289, 227 (1979).
6. P. Brix and H. Kopfermann, Z. Phys., 126, 344 (1949).
7. H. Hühnermann et al., Contributed papers, these proceedings.
8. W. Klempt, R. Neugart, F. Buchinger, A.C. Mueller, K. Wendt and C. Ekström, Contributed paper, these proceedings.
9. H.L. Ravn, Phys. Rep., 54, 201 (1979).
10. P. Hoff et al., to be published.
11. W.D. Myers, Phys. Lett., 30B, 451 (1969), see also Invited paper to these proceedings.
12. K. Heilig and A. Steudel, Atomic Data and Nuclear Data Tables, 14, 613 (1974).
13. S.E. Larsson, G. Leander and I. Ragnarsson, Nucl. Phys., A307, 189 (1978).
14. C. Ekström, Proc. 4th Int. Conf. on Nuclei far from Stability, Helsingør, 1981 (CERN 81-09, 1981), p. 12.
15. J. Rekstad and G. Løvhøiden, Nucl. Phys., A267, 40 (1976).
16. C. Ekström and I.-L. Lamm, Physica Scripta, 7, 31 (1973).
17. R.F. Casten, D.D. Warner, D.S. Brenner and R.L. Gill, Phys. Rev. Lett., 47, 1433 (1981).
18. E. Matthias et al., Contributed papers, these proceedings.
19. E.B. Shera, Invited paper, these proceedings.
20. R. Engfer, H. Schneuwly, J.L. Vuilleumier, H.K. Walter and A. Zehnder, Atomic Data and Nuclear Data Tables, 14, 509 (1974).
21. C.W. de Jager, H. de Vries and C. de Vries, Atomic Data and Nuclear Data Tables, 14, 479 (1974).
22. S.L. Kaufman, Opt. Commun., 17, 309 (1976)
23. K.-R. Anton, S.L. Kaufman, W. Klempt, G. Moruzzi, R. Neugart, E.W. Otten and B. Schinzler. Phys. Rev. Lett., 40, 642 (1978).